RSC Advances

PAPER

View Article Online
View Journal | View Issue

Cite this: *RSC Adv.*, 2015, **5**, 70874

Reactivity of iron-based nanoparticles by green synthesis under various atmospheres and their removal mechanism of methylene blue†

Jiewen Lin,[a] Xiulan Weng,[b] Xiaoying Jin,[b] Mallavarapu Megharaj,[c] Ravi Naidu[c] and Zuliang Chen*[bc]

Received 8th June 2015
Accepted 10th August 2015

DOI: 10.1039/c5ra10629j

www.rsc.org/advances

In this study, iron-based nanoparticles (Fe NPs) were synthesized using tea extracts under various atmospheres (N_2, O_2 and air) to understand how atmospheres impact on the reactivity of Fe NPs, where Fe NPs were used for the degradation of methylene blue (MB). SEM and FTIR confirmed the morphology and change in size of iron-based nanoparticles before and after reaction with MB, indicating that different Fe composition, morphology and size were obtained under various atmospheres resulting in different reactivity of Fe NPs. In addition, various parameters impacting on removing MB by Fe NPs synthesized under various atmospheres show that the solution pH significantly affects the reactivity of Fe NPs. Furthermore, the data fitted well to the pseudo-second-order adsorption and pseudo-first-order reduction models, confirming that the removal of MB was based on both adsorption and reduction. Langmuir and Freundlich isotherms demonstrate that the removal of MB by Fe NPs synthesized under various atmospheres was different due to their composition, morphology and size. Finally, the degraded products such as benzothiazole were identified by gas chromatography-mass spectrometry (GC-MS) after the degradation of MB, and finally a feasible removal pathway is proposed.

1. Introduction

Dyes are generally used in textiles, paper, tanneries and rubber manufacturing, and removing dye from discharge effluents remains a serious problem.[1] The dyes such as methylene blue (MB) released into the environment may cause an increase in chemical and biological oxygen demand, and it are difficult for microbes to decompose.[2] Since MB is a type of cationic dye with great stability, the degradation of MB by the methods such as biological, chemical precipitation and adsorption is difficult.[3] Activated carbon[4] and wheat shells were used to remove basic dye from aqueous solutions.[3]

Developments in nanotechnology have allowed iron nanoparticles (Fe NPs) to be the subject of increasing attention in the field of wastewater treatment containing dyes. The mechanisms for removing dyes and their dependence on adsorption and reduction by Fe NPs have been proposed. For instance, magnetic Fe_3O_4 nanoparticles were utilized for adsorption of neutral red dye from aqueous solution.[4] Nanoscale zero-valent iron (nZVI) supported bentonite was used to degrade acid violet red B.[5] To date, numerous methods have been developed for the synthesis of Fe NPs, and the chemical method of using sodium borohydride ($NaBH_4$) as a reducing agent is often employed in the synthesis of Fe NPs. Drawbacks in the chemical method include low production rates, high energy consumption, and high cost, as well as contamination arising from chemical precursors, toxicity of the used solvents and generation of hazardous by-products.[6,7] In contrast, the green synthesis of metal nanoparticles using plant extracts due to the ability of polyphenols to function as natural reducing agents has been proposed as an alternative to the chemical method.[7] Hence, synthesis of metal nanoparticles using plant extracts is generally cost-effective, biocompatible, non-toxic, and eco-friendly.[6,7]

In developing the green synthesis of Fe NPs, only a few studies have been done using plant extracts for synthesis of Fe NPs. Consequently, there are limitations in understanding the effect of synthetic conditions on the morphology and size distribution of Fe NPs, which involve the reactivity of Fe NPs. In this paper, iron-based nanoparticles synthesized by green tea extracts passing N_2, O_2 and air and their used for the removal of MB in aqueous solution were investigated. In addition, we particularly investigate the mechanism for removing MB using kinetic studies. Thus, the following aspects were done: (1) characterization of Fe NPs synthesized under N_2 (N–Fe NPs), O_2

[a]*School of Chemistry and Chemical Engineering, Fujian Normal University, Fuzhou 350007, Fujian Province, China*

[b]*School of Environmental Science and Engineering, Fujian Normal University, Fuzhou 350007, Fujian Province, China. E-mail: Zuliang.chen@newcastle.edu.au; Tel: +61-02-49139748*

[c]*Global Centre for Environmental Remediation, University of Newcastle, Callaghan, NSW 2308, Australia*

† Electronic supplementary information (ESI) available. See DOI: 10.1039/c5ra10629j

(O–Fe NPs) and air (air–Fe NPs) before and after reaction with MB to understand their differences in morphology and size, (2) the reactivity of Fe NPs synthesized under N_2, O_2 and air by estimation of various experimental parameters affecting the removal of MB; (3) the study of adsorption and reduction kinetics to further understand the removal process of MB and proposing a feasible removal mechanism.

2. Experimental

2.1. Preparation of Fe NPs (N_2, O_2 and air)

The extract of green tea was prepared by adding 60 g of processed green tea leaf into 1000 mL distilled water in a water bath heated at 353 K for 1 h. Then the extracts were taken for vacuum filtration after cooling to room temperature. Before 0.10 mol L^{-1} Fe_2SO_4 was added to the tea extracts with a ratio volume of 1 : 2, we passed it into the N_2, O_2 or air and kept it in a ventilation state during the synthetic process. Following vacuum-filtration this mixture's complete reaction was taken to the vacuum drying chamber for 12 h. Only then were these nano-solid particles used to remove MB.

2.2. Characterization

Scanning electron microscopy (SEM) images of GT-Fe NPs synthesized under N_2, O_2 and air before and after reaction with MB were acquired using a JSM-7500F (JEOL Ltd Co., Tokyo, Japan) to observe the surface morphology and size. The spectrum of MB, green tea extract, and Fe NPs inletting N_2, O_2 and air before and after reaction with MB were determined by Fourier transform infrared spectroscopy (FTIR Nicolet 5700, Thermo Corp., USA). A 1% specimen was mixed with 100 mg KBr to press into a sheer slice so that any changes in the functional groups before and after reaction could be observed.

The MB degradation products were characterized by gas chromatography-mass spectrometry (GC-MS, Thermo Corp., USA). The analytical conditions are listed as follows: ethyl acetate as solvent; capillary column (30 mm) as separation; helium as carrier gas and the sample volume set at 270 °C. The temperature programs were determined since the initial temperature was 50 °C for 2 min and then programmed to increase by 30 °C per minute up to 220 °C and then hold at 220 °C for 3 min. Then temperature was increased up to 260 °C by 6 °C per minute for 10 min holding. The mass spectrometry starts from 20 to 600 (m/z).

2.3. Batch experiments

To compare the removal efficiency of MB in aqueous solution, the degradation experiments were carried out using Fe NPs (0.03 g) synthesized under N_2, O_2 and air synthesized added to 30 mL MB at diverse conditions. Mixed solutions were stirred on a rotary shaker (125 rpm) at 298 K to various time intervals, then centrifuged at 7000 rpm for 5 min. The influence of experiment parameters on the removing MB was investigated. For instance, dosage of Fe NPs was 0.5–2 g L^{-1} in this study, initial concentration of MB was 50–100 mg L^{-1}, the reaction temperature was 298–313 K, and solutions of pH values ranged from 3.03–9.44. Experiments were carried out in duplicate. The removal efficiency of MB using N–Fe NPs, O–Fe NPs and air–Fe NPs *vs.* the time (5, 10, 20, 30, 40, and 50 min) at the temperature of 293 K, 298 K, 303 K and 313 K, respectively were showed in Fig. S1.† The various kinetic parameters were obtained from fitting the concentration of MB *vs.* the time. To investigate the stability of the Fe NPs, the recyclable experiments were conducted at the optimum condition of $T = 313$ K, $C_0 = 50$ mg L^{-1}, $C = 1$ g L^{-1} and pH = 9.44 for three times, and the results were showed in Fig. S2.†

UV-visible Spectrophotometer (722 N, Shanghai, China) was used to detect the concentration of MB solution at λ_{max} = 665 nm (Fig. S3†). The efficiency in removing MB was calculated using the following equation.[6]

$$\eta = \frac{C_0 - C_t}{C_0} \quad (1)$$

where η (%) represents the MB removal percentage, and C_0 and C_t (mg L^{-1}) represent the concentration of MB at initial and t time, respectively.

3. Results and discussion

3.1 Characterization

3.1.1 SEM analysis. The morphology and size of N–Fe NPs, O–Fe NPs and air–Fe NPs are observed in Fig. 1. The images of in Fig. 1(a), (c) and (e) show Fe NPs (N_2, O_2 and air) before reaction with MB, respectively, which confirm that the Fe NPs have a spheroid morphology. The size of N–Fe NPs, O–Fe NPs and air–Fe NPs is 87.4, 141.2 and 117.8 nm, respectively. This is because it is difficult to oxidize Fe^0 in N_2 atmosphere hence the sizes of N–Fe NPs are smallest which agrees with the following analysis of FTIR. Additionally, the images of in Fig. 1(b), (d) and (f) present Fe NPs (N_2, O_2 and air) after reaction with MB. It can be observed that the surface of Fe NPs became scabrous when they gathered into clusters and the sizes of N–Fe NPs, O–Fe NPs and air–Fe NPs were determined as being 131.9, 271.2 and 182.4 nm, respectively. This is due to: (1) iron oxide and hydroxide (Fe_3O_4, Fe_2O_3, Fe $(OH)_3$ and Fe(OOH)) forming on the surface of Fe NPs after their reaction with MB;[8] and (2) MB molecules or degraded products were adsorbed onto the Fe NPs' surface.

3.1.2 FTIR analysis. The results of FTIR are shown in Fig. 2, which represent Fe NPs (N_2, O_2 and air) before and after reaction with MB, green tea extract and MB powder. As shown in Fig. 2(a), (c) and (e), the bands around 1629 cm^{-1}, which are attributed to the stretching vibration of the C=C groups of organics of green tea extract, reflect the higher carbohydrate content of all the fresh Fe NPs. The band at approximately 1337 cm^{-1} corresponds to the asymmetric vibration of the C_{Ar}–N–CH_3 (ref. 9) and the band at approximately 765 cm^{-1} corresponds to the Fe–OH vibration. Compared to the FTIR spectra of the fresh Fe NPs (Fig. 2(a), (c) and (e)), the change in the bands for used Fe NPs is observed in Fig. 2(b), (d) and (f). As shown in Fig. 2(b), (d) and (f), the bands at around 827 cm^{-1} correspond to the =C–H plane bending vibration on benzene which were also detected in Fig. 2(h), indicating that the MB molecules were adsorbed onto the surface of Fe NPs (N–Fe NPs, O–Fe NPs and air–Fe NPs).[9]

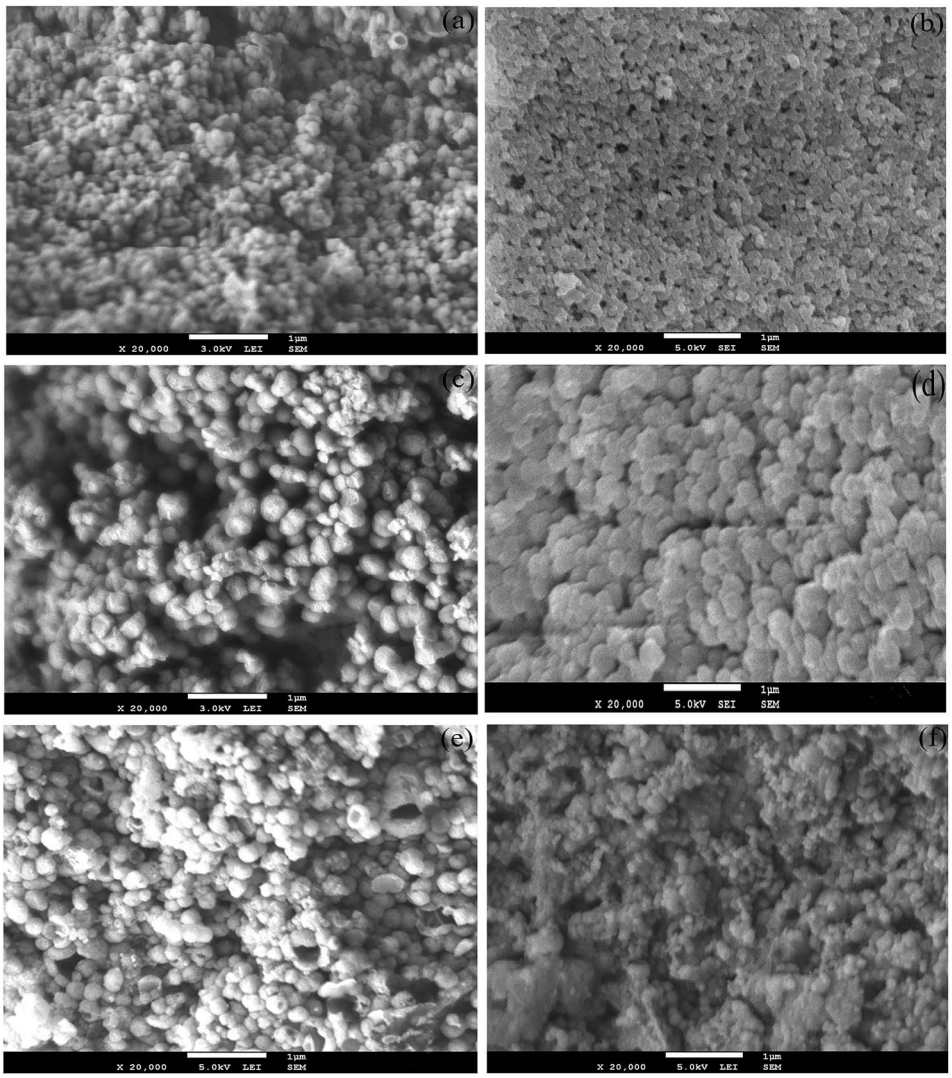

Fig. 1 SEM images of N–Fe NPs before (a) and after (b) reaction with MB; O–Fe NPs before (c) and after (d) reaction with MB; air–Fe NPs before (e) and after (f) reaction with MB.

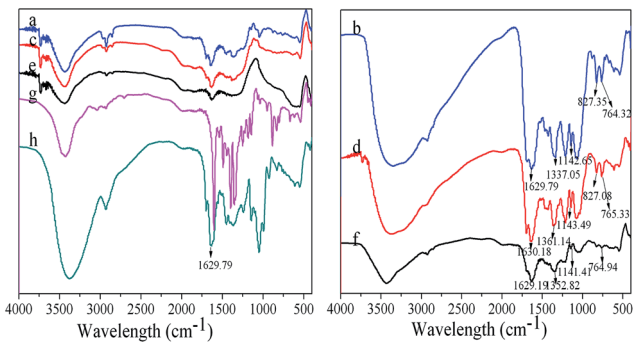

Fig. 2 FTIR spectra of N–Fe NPs before (a) and after (b) reaction with MB; O–Fe NPs by pass before (c) and after (d) reaction with MB; air–Fe NPs by before (e) and after (f) reaction with MB; green tea extract (g); MB powder (h).

There were strong bands at 1337–1361 cm^{-1} referring to C_{Ar}–N (stretching between aromatic ring and nitrogen atom) and CH_3 asymmetric vibration, the N–CH_3 stretching at 1143 cm^{-1}. These were all attributable to MB or its degraded products. The bands at approximately 764 cm^{-1} were C–H out of plane bending vibration on benzene, which probably corresponded to the degraded products of MB by Fe NPs. The adsorption band at 1630 cm^{-1} signified the C=C stretching vibration[9] and was shifted subtly to broadly imply that MB was most likely adsorbed onto the surface of Fe NPs (N_2, O_2 and air).

When comparing the differences in Fig. 2(b), (d) and (f), which represents the degradation of MB by N–Fe NPs, O–Fe NPs and air–Fe NPs, respectively, the wavelength of various functional groups shifting to longer wavelength on O–Fe NPs is observed. However, the high band intensity indicates that the MB molecules are adsorbed onto the surface of Fe NPs, yet on the other hand, the degraded products reduced by Fe NPs are capped simultaneously on the surface.[7,8] Additionally, it emerged that the intensity of band corresponded to N–Fe NPs more strongly than the O–Fe NPs and air–Fe NPs. This is due to the fact that the MB molecules on the surface of N–Fe NPs were reduced by Fe^0, resulting in the surface active sites being

unsaturated and more MB molecules adsorbed. The mentioned above results from FIIR provide the evidence for the removal of MB based on the both adsorption and reduction.[8]

3.2 The effect of various parameters on removing MB

3.2.1 Effect of initial pH values. The initial pH value is one of the most significant parameters influencing the removal process of dyes for water treatment since the charge of surface on adsorbent and dye molecules can be influenced by pH values in aqueous solution.[10,11] As shown in Fig. 3(a), the efficiency in removing MB by N–Fe NPs, O–Fe NPs and air–Fe NPs was improved when the pH range increased from 3.03 to 9.44. This is due to the surface active sites of Fe NPs (N_2, O_2 and air) transforming from positive to negative charge when pH increased, resulting in the presence of electrostatic attraction between the adsorbents and MB molecules since MB molecule is intrinsically cationic dyes. In contrast, Fe^0 can be corroded to form maghemite (γ-Fe_2O_3), magnetite (Fe_3O_4) and iron hydroxides.[6] On the other hand, we can conclude that the effect of removing MB by N–Fe NPs (91.5%) was better than that of O–Fe NPs (76.6%) and air–Fe NPs (83.9%) at pH = 9.44. The is due to the fact that Fe^0 occupying most of the internal structure of N–Fe NPs while iron oxide nanoparticles occupied the main parts of the surface of both O–Fe NPs and air–Fe NPs.

3.2.2 Effect of dosage of Fe NPs. The effect of Fe NPs dosage on the removal of MB *via* Fe NPs (N_2, O_2 and air) is presented in Fig. 3(b), where we can observe that increasing the amount of adsorbent (range from 0.5–2.0 g L^{-1}) enhanced the dye removal efficiency. This is attributed to the larger iron surface area and more available adsorption active sites.[10] Moreover, the adsorption capacity of Fe NPs increases when the absorbent dosage also increases. As shown in Fig. 3(b), when the amount of adsorbent increases to 2.0 g L^{-1}, the removal efficiency of MB using Fe NPs (N_2, air and O_2) reach 100.0%, 97.0% and 78.2% respectively. It can be seen that the N–Fe NPs were the most efficient in removing MB compared to the others, contributing to the presence of zero-valent iron nanoparticles. Moreover this finding is consistent with the above conclusion.

3.2.3 Effect of initial concentration of MB. The effect of initial dye concentration in solution on the efficiency in removing MB is documented in Fig. 3(c). As the initial MB concentration increases from 50 to 100 mg L^{-1}, the percentage of MB removed by N–Fe NPs declines from 97.4% to 55.6%, while that by O–Fe NPs slowing down markedly from 83.0% to 32.5% and that by air–Fe NPs is between them. The removal efficiency of dye decreased when dye concentration increased, because there were less available surface active sites for constant adsorbent dosage. Furthermore, mass-transfer resistance inhibited MB molecules being adsorbed onto the surface of Fe NPs from solution phase.[11] However, the presence of Fe^0 in N–Fe NPs led to the difference with O–Fe NPs and air–Fe NPs in terms of efficiently removing MB. Therefore we can conclude that N–Fe NPs are the most efficient in removing MB.

3.2.4 Effect of temperature. Temperature plays an important role in influencing the removal efficiency of adsorption and reduction process for MB by Fe NPs (N_2, O_2 and air). The effect of reaction temperature (293 K, 298 K, 303 K and 313 K) on the removal efficiency using Fe NPs is depicted in Fig. 3(d). Here, the efficiency of N–Fe NPs in removing MB was 51.4, 87.3, 89.4

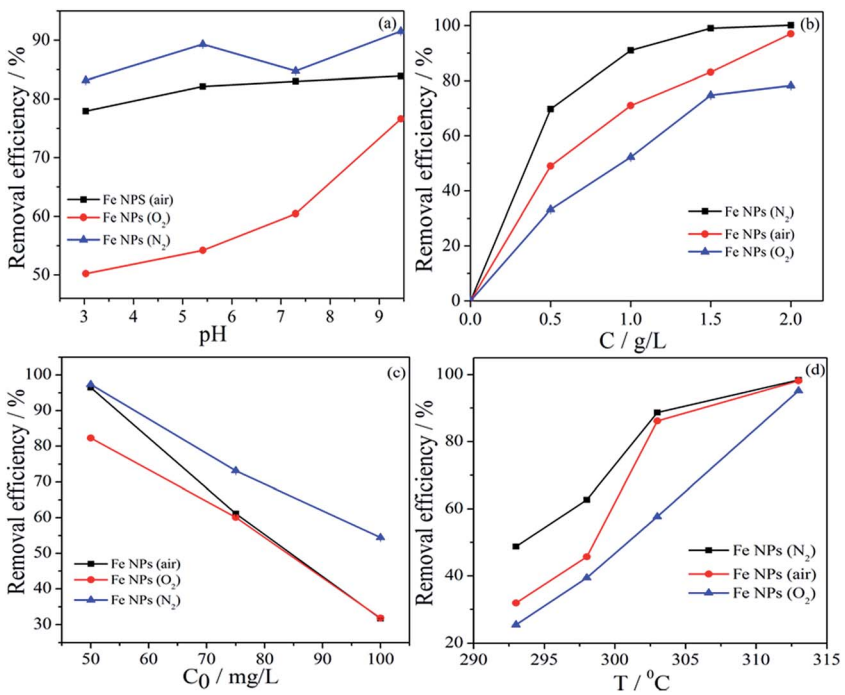

Fig. 3 Degradation of MB at experiment parameters. (a) Effect of the initial pH values. Condition: 1.0 g L^{-1}; 50 mg L^{-1}; 30 mL; 298 K; 125 r min^{-1}; (b) effect of dosages of Fe NPs (N_2, O_2 and air). Condition: pH = 7.3; 50 mg L^{-1}; 30 mL; 298 K; 125 r min^{-1}; (c) effect of initial concentration of MB. Condition: pH = 7.3; 1.0 g L^{-1}; 30 mL; 298 K; 125 r min^{-1}; (d) effect of temperature. Condition: pH = 7.3; 1.0 g L^{-1}; 30 mL; 50 mg L^{-1}; 125 r min^{-1}.

and 98.4%, at temperatures of 298, 293, 303 and 313 K, respectively. It is indicated that the removal of MB by N–Fe NPs was an endothermic process. However, as shown in Fig. 3(d), the removal efficiency of MB by O–Fe NPs was 25.4, 39.5, 57.7, and 95.2% at temperatures of 293, 298, 303 and 313 K, respectively. It is suggested that the O–Fe NPs were less efficient in removing MB compared to N–Fe NPs because the surface of O–Fe NPs was covered with iron oxide and hydroxide. Meanwhile, the air–Fe NPs' efficiency when removing MB was determined by the amount of nZVI and iron oxide nanoparticles these particles contained. Consequently, the efficiency in removing dyes can be boosted by raising the temperature because this serves to encourage collisions between MB molecules, which in turn lead to more activation energy.[12] Homologous phenomena have been reported in some studies.[10,13] Moreover, this result agrees with the kinetic study which is reported below.

3.3 Kinetic study

Previous reports[14,15] have indicated that MB removal by Fe NPs involves adsorption and reduction. However, to further confirm the removal of MB based on adsorption and reduction, adsorption and reduction kinetics, adsorption isotherms and thermodynamic models were used to fit the data. The amount of absorbed MB was calculated using the following formula:[15,16]

$$q_e = \frac{(C_i - C_e)V}{m} \quad (2)$$

where q_e (mg g^{-1}) represents the amount of MB absorbed by Fe NPs at equilibrium, C_i (mg L^{-1}), the concentration of MB in solution at time t, C_e (mg L^{-1}), the equilibrium concentration of MB in solution, V (mL), the volume of MB solution used and m (g) is the weight of the adsorbent used.

3.3.1 Adsorption kinetics. The adsorption of MB onto Fe NPs synthesized under various atmospheres may involve physical and chemical sorption. The dynamic process of MB adsorption was analyzed by using pseudo-first-order and pseudo-second-order equations, because these kinetic models are often applied to fit the process of adsorption. Pseudo-first-order equation is described as follows:[17]

$$\ln(q_e - q_t) = \ln q_e - k_1 t \quad (3)$$

where q_e (mg g^{-1}) is the number of MB molecules absorbed onto the absorbent at equilibrium, q_t (mg g^{-1}) is the amount absorbed at time t and k_1 (min^{-1}) is the rate constant of pseudo-first-order adsorption that can be calculated from the slope of linear plot of $\ln(q_e - q_t)$ *versus* t.

The linear kinetic equation of pseudo-second-order can be given as follows:[17]

$$\frac{t}{q_t} = \frac{1}{k_{ps} q_e^2} + \frac{t}{q_e} \quad (4)$$

where q_e and q_t (mg g^{-1}) correspond to adsorption capacities at equilibrium and time, respectively; and k_{ps} (g mg^{-1} min^{-1}) is the rate constant of pseudo-second-order adsorption equation that can be obtained by calculating the intercept of the linear equation.

The kinetic parameters, correlation coefficients (r^2) and rate constant (k), of pseudo-first-order and pseudo-second-order models, were calculated from eqn (3) and (4). As shown in Table 1, the r^2 was more than 0.896 which indicated that the adsorption of MB by N–Fe NPs, O–Fe NPs and air–Fe NPs all suited the pseudo-second-order model. Compared to the pseudo-first-order model, the coefficient values for the pseudo-second-order model ranged from 0.89–1.00 for the N–Fe NPs. This indicated that the sorption process mainly involved chemisorption. Meanwhile the rate constant also rose as T increased (the range of k_2 was 0.03–48.24), implying the adsorption of MB may be an endothermic process, which further proved that temperature had a significant impact on the rate constant. The correlation coefficients (r^2) of pseudo-first-order in the range from 0.45–0.97 for O–Fe NPs, were less than that of pseudo-second-order (the range of r^2 was 0.98–0.99), confirming that the sorption of MB onto O–Fe NPs fitted well with to the pseudo-second-order model.

However, the pseudo-first-order model can be also used to describe the adsorption process with O–Fe NPs comparing to N–Fe NPs at 313 K, implying the adsorption capacity of O–Fe NPs was stronger due to the contents of iron oxide nanoparticles. Furthermore, the adsorption capacity of air–Fe NPs may lie between N–Fe NPs and O–Fe NPs, which will be further proven by Langmuir isotherms models. The adsorption process of MB by various adsorbents has been reported previously[11,17] Furthermore all the experimental data showed that the adsorption process of MB fitted well to the pseudo-second-order model, and it occurred through chemisorption rather than physical adsorption.

3.3.2 Reduction kinetics. The process of removing MB by Fe NP (N_2, O_2 and air) includes not only chemical adsorption, but may also involve chemical reaction. Therefore, reduction

Table 1 Adsorption kinetics parameters for the removal of MB by Fe NPs (N_2/O_2/air)

	Pseudo-first-order model		Pseudo-second-order	
Temp (K)	k_1 (min^{-1})	r^2	k_2 (g mg P^{-1} min^{-1})	r^2
N_2				
293	0.2055	0.7759	0.0261	0.8961
298	0.0598	0.8900	1.8029	0.9987
303	−0.0261	0.4054	0.8343	0.9997
313	0.0041	0.0100	48.3139	1.0000
O_2				
293	0.0521	0.4515	0.2584	0.9836
298	0.0859	0.8493	0.1751	0.9876
303	0.1003	0.8871	0.0462	0.9879
313	0.0527	0.9751	0.0721	0.9990
Air				
293	0.0464	0.94	0.6589	0.9988
298	0.0360	0.9012	0.9546	0.999
303	0.0299	0.8317	0.1479	0.9588
313	0.0949	0.952	1.4292	1.0000

Table 2 Reduction kinetics parameters for the removal of MB by Fe NPs (N_2/O_2/air)

	Pseudo-first-order		Pseudo-second-order	
Temp (K)	k_1 (min^{-1})	r^2	k_2 (g mg P^{-1} min^{-1})	r^2
N_2				
293	0.0085	0.7589	0.0035	0.8732
298	0.0052	0.9039	0.0024	0.9179
303	0.0058	0.8775	0.0105	0.8583
313	0.0063	0.9252	0.0636	0.8971
O_2				
293	0.0027	0.7468	0.0006	0.7371
298	0.0037	0.9174	0.0013	0.9576
303	0.0107	0.9563	0.004	0.9668
313	0.0405	0.9735	0.0424	0.9703
Air				
293	0.0014	0.9426	0.0004	0.9463
298	0.0015	0.9685	0.0005	0.9670
303	0.0243	0.8706	0.0188	0.7742
313	0.0404	0.8668	0.1960	0.9617

kinetics was investigated to further understand the removal process. Pseudo-first-order and pseudo-second-order models were provided as shown below:[18]

$$\ln\frac{C}{C_0} = -k_{obs}t \quad (5)$$

$$\ln\left(\frac{1}{C_t} - \frac{1}{C_0}\right) = kt \quad (6)$$

where k_{obs} and k correspond to the pseudo-first and pseudo-second-order rate constants, respectively. C_0 and C_t present the initial and instantaneous concentration of MB in aqueous solution at $t = 0$ and $t = t$.

As shown in Table 2, with reference to the N–Fe NPs, values of the regression coefficients (r^2) of the pseudo-second-order model ranged from 0.8583 to 0.8971. However, the pseudo-first-order model indicated that regression coefficients (r^2) ranged from 0.7589 to 0.9252, illustrating the reduction process of MB fitted well to pseudo-first-order kinetics. Associated with the above finding, it can be concluded that the process of removing MB by N–Fe NPs may involve chemical reaction, due to there being much more zero-valent iron nanoparticles (nZVI) in N–Fe NPs than in O–Fe NPs, where the degraded products was proven by GC-MS analysis. Values of the regression coefficients (r^2) of O–Fe NPs are demonstrated in Table 2. They range from 0.7468 to 0.9735 in the pseudo-first-order kinetic model and 0.9382 to 0.9703 for the pseudo-second-order kinetic model. It indicates that the pseudo-second-order model can describe the kinetic process more properly.

The removal of MB by O–Fe NPs was a more complicated process, as proven by SEM, there was a thick layer of iron oxide nanoparticles on the surface of O–Fe NP. Firstly, the MB molecules were transferred from liquid to solid *via* electrostatic interaction and π–π interaction of species groups between adsorbate–adsorbent.[19] Then, MB molecules were adsorbed into the interface of O–Fe NPs due to the presence of adsorption sites. Lastly, adsorbed molecules that made contact with nZVI were then reduced by O–Fe NPs. Nevertheless, the restored strength was relatively weak because there was little nZVI content. Consequently, the results for reduction kinetics demonstrated that the degradation of MB by N–Fe NPs was more efficient than that of O–Fe NPs and air–Fe NPs.

3.4 Adsorption isotherms

To further analyze the process of adsorption, the Langmuir and Freundlich isotherm models were employed to fit the experimental data. The Langmuir adsorption isotherm assumes that adsorbents' surface sites are homogeneous and the adsorption process is a monolayer adsorption. It has been successfully used for describing the dynamic process of adsorption. The linear equation of the Langmuir model is given as follows:[20]

$$\frac{C_e}{q_e} = \frac{1}{q_{max}K_L} + \frac{C_e}{q_{max}} \quad (7)$$

where C_e (mg L^{-1}) is the equilibrium concentration of MB solution; q_e (mg g^{-1}) represents the amount absorbed at equilibrium; q_{max} (mg g^{-1}); and K_L (L mg^{-1}) corresponds to the maximum adsorption capacity and the Langmuir constant or equilibrium constant that can be calculated from the slope and intercept of the linear regression C_0/q_e *versus* C_e.

The linear equation of the Freundlich isotherm, which is an empirical formula and describes the adsorption that takes place on the heterogeneous surface of an adsorbent, can be shown as follows:[20]

$$\log q_e = \log K_F + \frac{1}{n}\log C_e \quad (8)$$

where C_e and q_e represent the equilibrium concentration of MB in aqueous solution and the equilibrium adsorbed. K_F and $1/n$ are the Freundlich constants, which relate to adsorption

Table 3 Isotherm parameters for the removal of MB by Fe NPs (N_2/O_2/air)

	Langmuir			Freundlich			
Parameters	q_{max} (mg g^{-1})	K_L (L mg^{-1})	r^2	K_F (L mg^{-1})	n (g L^{-1})	r^2	R_L
N_2	52.9100	0.7975	0.9931	45.5407	37.4531	0.3897	0.03–0.31
O_2	28.3286	0.2822	0.9908	37.2992	−21.367	0.2131	0.05–0.16
Air	28.7356	0.3207	0.9906	56.5588	−6.8540	0.9613	0.04–0.46

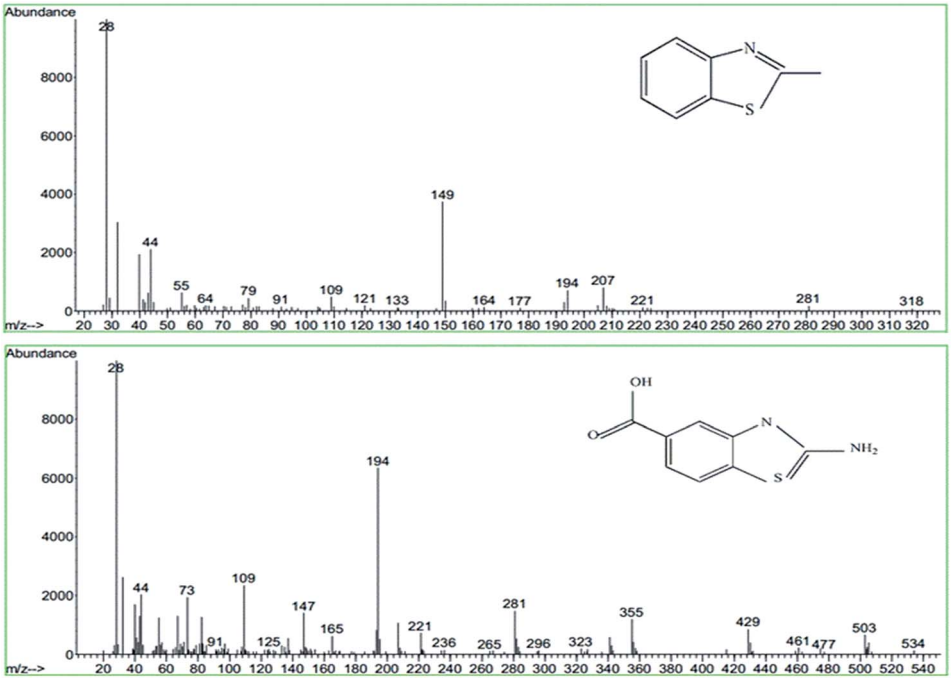

Fig. 4 Mass spectrometer of degraded products.

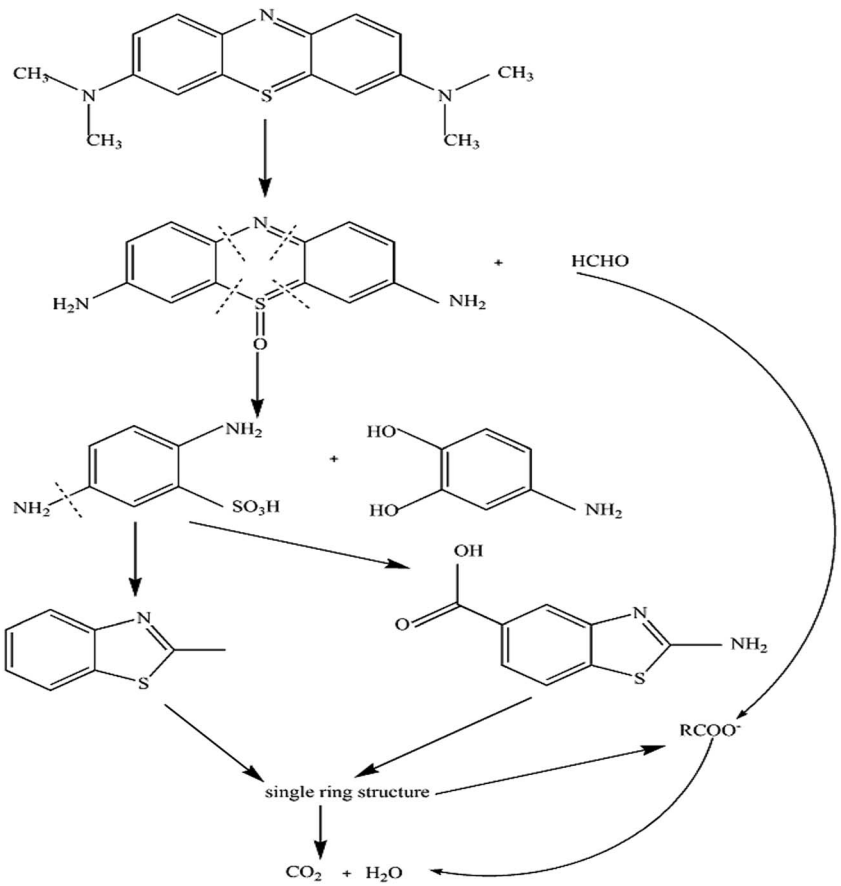

Fig. 5 The reduction degradation pathway of MB molecules.

capacity and adsorption intensity, respectively. K_F was generally used to describe the strength of the relationship between adsorbate and adsorbent.[21] The values of n in the 1 to 10 range represent good adsorption, indicating that this process favored adsorption.

All the parameters values are summarized in Table 3 in terms of eqn (7) and (8). The adsorption isotherm is critical for investigating the adsorption system, which describes the correlation between adsorbate and adsorbent. As shown in Table 3, the r^2 values were all higher than 0.99, indicating the adsorption of MB by N–Fe NPs and O–Fe NPs fitted well to the Langmuir isotherm equation. The values illustrated that the N–Fe NPs or O–Fe NPs' adsorption of MB was a monolayer process due to the homogeneous active sites on the surface of Fe NPs. The Langmuir adsorption isotherm equation hypothesized that the adsorbents' surface active sites were homogeneous and had identical energy. Furthermore the active sites were saturated when monolayer molecules were adsorbed onto the adsorbent surface. The maximum adsorption capacity q_{max} for MB onto N–Fe NPs and O–Fe NPs was obtained from the slope of the linear equation and the values shown in Table 3 were 52.910 and 28.329, respectively. Thus the adsorption strength of N–Fe NPs for MB was higher than O–Fe NPs due to reduction of NZVI. The Freundlich exponents (r^2 = 0.3897 and 0.2131, respectively) were less than that of Langmuir, confirming that the Freundlich adsorption isotherms model did not properly fit the MB adsorption process.

The values of dimensionless constant separation factor (R_L) can be calculated using the following equation,[21] which is another essential parameter of the Langmuir isotherm:

$$R_L = \frac{1}{(1 + bC_i)} \quad (9)$$

The results of R_L given in Table 3 were $1 > R_L > 0$ for the adsorption of MB onto N–Fe NPs (in the 0.03–0.31 range) and O–Fe NPs (in the 0.05–0.16 range), demonstrating the adsorption process for MB was favorable.[22]

3.5 Degraded products analysis

The degradation products of MB using Fe NPs (N_2, O_2 and air) were conducted by GC-MS analysis, and the results were shown in Fig. 4(a) and (b), respectively. A possible degradation pathway of MB using Fe NPs is illustrated in Fig. 5. Analogues of benzothiazole were detected in the degradation, a phenomenon that has been documented previously.[23,24] As shown in Fig. 4, the signals at m/z = 149 and m/z = 194 correspond to intermediates after the structure of the MB molecules broken into smaller molecules components. As shown in Fig. 5, a possible degradation process is as follow. Firstly, Cl^- is ionized in aqueous solution, then the loss of four $-CH_3$ connected to N proceeds, which has a smaller bond dissociation energy (BDE) value in the MB molecular structure.[23] Secondly, the $-CH_3$ turns into HCHO or $RCOO^-$. Thirdly, the C–S and C–N bonds in the middle ring which are the more active parts are broken into other small molecular weight intermediates. Finally, all the organic degradation products are transformed into CO_2 and H_2O, and these may contain inorganic ions, such as Cl^-, SO_4^{2-} and NO_3^- in solution.

4. Conclusions

This study has demonstrated that green synthesis Fe NPs under various atmospheres (N_2, O_2 and air) can be used to remove MB due to its reduction by Fe^0 nanoparticles and adsorption on iron oxide nanoparticles. SEM and FTIR analyses showed that iron oxides were formed through the corrosion of Fe in oxygen and air atmosphere. Moreover, temperature had a significant influence on the removal of MB. It indicated that the degradation process of MB by N–Fe NPs, O–Fe NPs and air–Fe NPs was an endothermic reaction. The investigation of kinetics demonstrated the degradation process of MB by N–Fe NPs fitted well to the pseudo-second-order adsorption and pseudo-first-order reduction models. It was a chemisorption process rather than a physical sorption one. While the degradation process of MB using O–Fe NPs and air–Fe NPs seemed to fit well to pseudo-second-order adsorption and reduction kinetics. Meanwhile, the Langmuir isotherm model proved that the degradation reaction had a homogeneous and monolayer adsorption character. Finally, the degraded products obtained from MB reacting with Fe NPs were identified by GC-MS analysis, and a possible degradation pathway of MB using Fe NPs is proposed.

Acknowledgements

The authors thank the financial support given by the National Natural Science Foundation of China (No. 41401585).

References

1 S. Dutta, A. Bhattacharyya, A. Ganguly, S. Gupta and B. Srabanti, *Desalination*, 2011, **275**, 26–36.
2 M. Iram, G. Chen, Y. P. Guan, A. Ishfaq and H. Z. Liu, *J. Hazard. Mater.*, 2010, **181**, 1039–1050.
3 T. X. Wu, N. T. Li, J. C. Zhao, H. Hidaka and N. Serpone, *Environ. Sci. Technol.*, 1999, **33**, 1379–1387.
4 A. Ghauch, A. Tuqan and H. A. Assi, *Environ. Pollut.*, 2009, **157**, 1626–1635.
5 Y. M. Lin, Z. X. Chen, Z. L. Chen, M. Megharaj and R. Naidu, *Appl. Clay Sci.*, 2014, **93–94**, 56–61.
6 X. L. Weng, L. L. Huang, Z. L. Chen, M. Megharaj and R. Naidu, *Ind. Crops Prod.*, 2013, **51**, 342–347.
7 S. Iravani, *Green Chem.*, 2011, **13**, 2638–2650.
8 L. L. Huang, X. L. Weng, Z. L. Chen, M. Megharaj and R. Naidu, *Spectrochim. Acta, Part A*, 2014, **117**, 801–804.
9 Z. Q. Yu and S. S. C. Chuang, *J. Phys. Chem. C*, 2007, **111**, 13813–13820.
10 Y. Bulut and H. Aydın, *Desalination*, 2006, **194**, 259–267.
11 F. L. Fu, D. D. Dionysiou and H. Liu, *J. Hazard. Mater.*, 2014, **267**, 194–205.
12 H. I. Chieng, T. Zehra and B. L. L. Linda, *Environ. Earth Sci.*, 2014, **46**, 1–15.

13 D. Kavitha and C. Namasivayam, *Bioresour. Technol.*, 2007, **98**, 14–21.
14 M. Auta and B. H. Hameed, *Chem. Eng. J.*, 2011, **175**, 233–243.
15 P. Sharma and R. M. Das, *J. Chem. Eng.*, 2013, **58**, 151–158.
16 A. Roy, B. Adhikari and S. B. Majumder, *Ind. Eng. Chem. Res.*, 2013, **52**, 6502–6512.
17 M. Auta and B. H. Hameed, *Chem. Eng. J.*, 2014, **237**, 352–361.
18 W. J. Jiang, C. Quan and X. Wei, *Environ. Sci. Technol.*, 2014, **50**, 1–27.
19 W. Chen, D. Lin and D. Q. Zhu, *Environ. Sci. Technol.*, 2007, **41**, 8295–8300.
20 S. Parimal, M. Prasad and U. Bhaskar, *Ind. Eng. Chem. Res.*, 2010, **49**, 2882–2888.
21 F. Tümsek and Ö. Avcı, *J. Chem. Eng. Data*, 2013, **58**, 551–559.
22 Z. X. Chen, T. Wang, X. Y. Jin and Z. L. Chen, *J. Colloid Interface Sci.*, 2013, **398**, 59–66.
23 F. M. Huang, C. Li, H. L. Wang and Z. C. Yan, *Chem. Eng. J.*, 2010, **62**, 250–256.
24 B. Yang, J. N. Zuo, X. H. Tang and F. L. Liu, *Ultrason. Sonochem.*, 2014, **21**, 1310–1317.